The Dynamic Structural Basis of Differential Enhancement of Conformational Stability by 5′- and 3′-Dangling Ends in RNA[†]

John D. Liu,[‡] Liang Zhao,[‡] and Tianbing Xia*

Department of Molecular and Cell Biology, The University of Texas at Dallas, Richardson, Texas 75083-0688

Received February 5, 2008; Revised Manuscript Received April 4, 2008

ABSTRACT: Unpaired bases at the end of an RNA duplex (dangling ends) can stabilize the core duplex in a sequence-dependent manner and are important determinants of RNA folding, recognition, and functions. Using 2-aminopurine as a dangling end purine base, we have employed femtosecond time-resolved fluorescence spectroscopy, combined with UV optical melting, to quantitatively investigate the physical and structural nature of the stacking interactions between the dangling end bases and the terminal base pairs. A 3′-dangling purine base has a large subpopulation that stacks on the guanine base of the terminal GC or UG pair, either intrastrand or cross-strand depending on the orientation of the pair, thus providing stabilization of different magnitudes. On the contrary, a 5′-dangling purine base only has a marginal subpopulation that stacks on the purine of the same strand (intrastrand) but has little cross-strand stacking. Thus a 5′-dangling purine does not provide significant stabilization. These stacking structures are not static, and a dangling end base samples a range of stacked and unstacked conformations with respect to the terminal base pair. Femtosecond time-resolved anisotropy decay reveals certain hindered base conformational dynamics that occur on the picosecond to nanosecond time scales, which allow the dangling base to sample these substates. When the dangling purine is opposite to a U and is able to form a potential base pair at the end of the duplex, there is an interplay of base stacking and hydrogen-bonding interactions that depends on the orientation of the base pair relative to the adjacent GC pair. By resolving these populations that are dynamically exchanging on fast time scales, we elucidated the correlation between dynamic conformational distributions and thermodynamic stability.

In large functional RNAs, e.g., rRNAs, about half of the nucleotides are involved in Watson−Crick or GU base pairing interactions within the double-stranded helical regions, where the average length of a continuous helix is approximately seven base pairs (*1*). Consequently, in a typical large RNA there are many helical ends where unpaired nucleotides are located. Unpaired nucleotides immediately adjacent to the terminal base pairs of a double helix (typically termed dangling ends) play an important role in RNA folding, recognition, and function. Examples include codon−anticodon interactions, recognition of tRNA acceptor stem, and, as revealed more recently, the mechanism of mRNA targeting via RNA interference-mediated pathways. Therefore, a deeper understanding of the thermodynamic, structural, and dynamic properties of these dangling ends in RNA will provide critical insights into their context-dependent functionality.

The thermodynamic effects of dangling ends have long been known since the early observations that RNA duplexes can be stabilized by the presence of dangling bases (*2–5*). Experimentally, it is straightforward to measure the extent of these stabilizing effects by directly comparing the stabilities of model duplexes with and without the dangling end bases, obtained from UV optical melting studies (*6*). Such studies have been typically conducted under high salt conditions, e.g., 1 M NaCl. The thermodynamic parameters of the stabilizing effects can then be derived within the framework of the nearest-neighbor model (*7, 8*), and they have been collected for a variety of sequence contexts (*7, 9*). Dangling ends are found to stabilize the core RNA duplexes through direct stacking interactions with the terminal base pair in a highly sequence-dependent manner, particularly for the 3′-dangling ends (*6, 10–13*). Base stacking interaction is the dominant force responsible for stabilizing nucleic acid structures for both helical and noncanonical regions and is one of the major considerations in RNA structure prediction from sequence information based on the first principles of thermodynamics (*1*); therefore, it is important to understand the context dependence of such stabilizing effects and its structural origin.

In general, a 3′-dangling base on terminal GC pairs provides more stabilization than on terminal AU pairs (*10, 13*), presumably due to the difference in the dipole moments between the two different Watson−Crick base pairs. In addition, larger purine bases can provide more stabilization than smaller pyrimidine bases as dangling ends (*4, 6, 10, 12, 13*), consistent with base stacking being the main source of stability enhancement. The orientation of the terminal pair is an important factor, as a 3′-A stacking on a CG pair, in the context of $^{CA3'}_{G}$, provides 1.7 kcal/mol stabilization,

[†] This work was supported in part by grants from the Robert A. Welch Foundation (Grant AT-1645) and THECB Norman Hackerman Advanced Research Program under Grant 009741-0004-2006.

* To whom correspondence should be addressed. E-mail: tianbing.xia@utdallas.edu. Phone: 972-883-6328. Fax: 972-883-2409.

[‡] These authors contributed equally to this work.

10.1021/bi800210t CCC: $40.75
Published on Web 05/06/2008

compared to 1.1 kcal/mol in the context of $^{GA3'}_{C}$. Increased interstrand stacking of the dangling base at the helical end seems to play a crucial role in determining the extent of the stabilization. It is remarkable that the presence of a 3′-A can even stabilize an RNA duplex with only two GC base pairs, and certain 3′-dangling ends can stabilize a duplex almost as much as a terminal Watson−Crick base pair (*5*). In particular, the 1.7 kcal/mol stabilization of $^{CA3'}_{G}$ is only slightly smaller than the Watson−Crick nearest-neighbor parameter of 2.1 kcal/mol for $^{CA3'}_{GU5'}$ (*7*). Most 5′-dangling ends, on the other hand, do not significantly stabilize an RNA core duplex (*2, 5*), typically less than 0.5 kcal/mol, no more than the effect of a 5′-phosphate group alone (*6, 7, 11, 12*). In addition, it has been proposed that the phosphate group that is 5′ to the terminal base pair (i.e., 3′ to the 5′-dangling base) restricts the conformation of the sugar and base of a 5′-dangling nucleotide (*6, 11*).

The stabilizing effects of dangling ends have been shown to be mostly enthalpic in nature, and specific solvation cannot account for these observations (*6, 10*), consistent with the notion that stacking is the dominant force responsible for the stabilization. The exact physical nature of base stacking interactions in nucleic acids is not fully understood, and a number of factors may contribute (*14*). Certain specific electrostatic interactions, e.g., between the O4 of U as a 3′-dangling end base and the amino group of C in the terminal CG pair ($^{CU3'}_{G}$), may account for the majority of the stabilization in that particular context (*15*). Modified bases or base analogues have been used to test this and other hypotheses on the nature of the stacking interactions involving the dangling end bases, including hydrophobicity, size of bases, and polarizability (*14–19*).

It has been proposed earlier that the presence of a dangling end base may promote more favorable stacking interactions among the internal base pairs in the duplex, which leads to enhanced stability (*3*). More recently, geometrical considerations in terms of stacking between the dangling end base and the adjacent terminal base pairs have been used to rationalize the experimental observations of the differential context-dependent stabilizing effects of dangling ends (*6, 10, 11*). For the A-form RNA duplex, a 3′-dangling base can stack directly on the terminal base pair and, in some cases, on the base of the opposite strand (*11*), thus helping to hold the duplex together. Evidence of the direct base stacking interaction between the duplex end and 3′-dangling base was obtained early on from NMR experiments on short RNA duplexes (*4, 5*). A 5′-dangling base, however, typically does not stack on the adjacent base pair (*11*), especially not on the base on the opposite strand, thereby providing little stabilization when compared to the 3′-dangling bases.

Dangling ends in DNA, as a comparison, have a range of stabilization that is smaller than that for dangling ends in RNA (*20*). The nature of the terminal base pair seems to be the major factor in determining the contribution by the dangling ends in DNA. Generally, larger purine bases provide more stabilizing effect than pyrimidine bases, similar to the RNA system (*16, 17, 20, 21*). As in the case of RNA, enthalpy also seems to be the origin of stability enhancement contributed by the dangling end. However, opposite to the trend observed for RNA, the 5′-dangling ends in DNA are generally more or equally stabilizing as 3′-dangling ends (*20, 22, 23*), although interesting exceptions to this general trend do exist (*20*). Presumably, the different trends between RNA and DNA dangling ends are due to the geometrical differences between the canonical A- and B-form duplexes (*11, 20, 23*). In DNA, a 5′-dangling base can more effectively stack on the terminal pair when compared to a 3′-dangling end in the B-form duplex (*23*).

A duplex may feature multiple dangling bases that may cooperatively stabilize the structure. For example, tRNAs contain a four-nucleotide single-stranded NCCA end 3′ to the acceptor stem that can stabilize the acceptor stem (*24*). In RNA, for dangling ends with more than one base, the largest contribution appears to come from the first dangling base, and the extra bases may add small additional stability (*5, 24–27*), but this effect was found to be dependent on the identity of the first dangling base (*26, 27*). The thermodynamics of longer dangling ends is relevant to small interference RNA-mediated gene regulation pathway, where double nucleotide 3′-dangling ends are present. In DNA, on the contrary, the length of dangling ends seems to have little effect (*25, 28, 29*).

These stabilizations measured in small RNA model systems correlate well with the positions of the dangling bases relative to the helical ends observed in the high-resolution structures of larger functional RNAs (*13, 15, 30*). Strongly stabilizing dangling ends (stabilization of more than 0.8 kcal/mol), e.g., $^{GA3'}_{C}$ and $^{CA3'}_{G}$, tend to be stacked on the adjacent terminal base pair in the context of these large RNAs, while weakly stabilizing ones (stabilization of less than 0.5 kcal/mol) are usually not stacked and are sometimes associated with turns in the backbone (*13, 15*). Therefore, the energetics of stabilization by dangling ends measured in small model systems is a good predictor of their stacking structural patterns in large RNAs. A more recent survey based on a more extensive set of structures revealed that the hydrogen bonds between the bases of the terminal pairs tend to be protected from solvent exchange by a stacked 3′-base which acts as a hydrophobic cap, effectively converting a terminal base pair into an internal pair, thereby reducing fraying, while a 5′-overhang provides little such protection (*30*). Therefore, the screening of the terminal base pair from solvent exchange correlates with the thermodynamic stabilization of dangling ends. This seems to be consistent with the partially preorganized direction-specific nearest-neighbor base stacking patterns found in single-stranded states of DNA and RNA (*31*). This type of correlation between the measured thermodynamic effects of dangling ends in small model systems and their relative locations with respect to the helical ends in large RNAs allows better prediction of both RNA secondary and tertiary structures (*1, 15*).

However, such correlations only relate a single observed static structure to the measured thermodynamics. RNA structures at various hierarchical levels are typically very dynamic on a wide range of length and time scales (*32*). In the case of dangling ends in RNA, it is unclear how dynamic these stacking structures are in different contexts, which may result in a distribution of stacked and unstacked substates. This raises the questions of whether the potentially heterogeneous distributions of stacking/unstacking conformations of dangling ends correlate with the differences in the observed context-dependent enhancement of duplex stabilities (*30*) and how the interplay of stacking and hydrogen-bonding interactions play a role in determining the dynamics.

Here we use a recently developed femtosecond dynamics strategy (*33*) to address these questions, with the aim of providing a dynamic structural basis for the sequence-dependent thermodynamic stability enhancements contributed by dangling ends in RNA. We demonstrate here that the observed context-dependent thermodynamic enhancement by dangling ends can be quantitatively rationalized by the dynamic heterogeneous population distributions of different stacking patterns, including inter- and intrastranded stacking and unstacked conformations, between the dangling end base and the terminal base pair. Such population distributions reflect the intrinsic flexibility of the dangling end bases that is strongly dependent on the context. Furthermore, the balance between base stacking interactions and hydrogen-bonding interactions involving the dangling bases plays an important role in determining the structure, stability, and dynamics of RNA structures.

EXPERIMENTAL PROCEDURES

Materials and UV Optical Melting. All of the RNA constructs were purchased from Dharmacon (Lafayette, CO) and were purified by PAGE. RNA concentrations were calculated from UV absorbance at 260 nm. The oligos were dissolved in a buffer of 100 mM NaCl, 20 mM sodium phosphate, and 0.2 mM Na_2EDTA, pH 6.5, unless otherwise noted, and annealed. UV optical melting experiments were performed on a Shimadzu 2401 UV spectrometer equipped with a temperature control module. Absorbance versus temperature melting curves were measured at 280 nm with a heating rate of 1.0 °C/min. Thermodynamic parameters were derived by van't Hoff analysis of a two-state model using the program Meltwin (*34*).

Femtosecond Time-Resolved Fluorescence Spectroscopy. Femtosecond pulses (110 fs, 800 nm, 2.3 mJ) are generated from a Ti:sapphire laser system (Spectra Physics). The pulse is split equally into two beams. One beam is directed to pump an optical parametric amplifier (OPA). The signal output from the OPA is quadrupled to generate the excitation pump pulse at 322 nm for 2-aminopurine. The remainder of the fundamental 800 nm is used as the probe pulse. The emission is collected by a pair of parabolic focus mirrors and mixed with the fundamental in the BBO crystal. The upconverted signal (257 nm, corresponding to 380 nm fluorescence) is detected by a photomultiplier after passing through a double-grating monochromator. RNA concentrations are 100 μM. All measurements were carried out at room temperature (22 °C) with the sample being constantly stirred during data collection. For experiments conducted under magic angle condition, the pump beam polarization is set at the magic angle (54.7°) with respect to the fluorescence polarization set by the BBO crystal, to avoid complications from orientational motions. The femtosecond transients were collected up to 400 ps and were analyzed using a least-squares fitting procedure, in which the multiexponential decays (three or four terms) were convoluted with a Gaussian response function with floating full width at half-maximum (fwhm)[1] (*35*). Parameter τ_4 is fixed at the average value (11.3 ns) of the observed lifetimes for free 2-aminopurine base, 9-methyl-2-aminopurine, and 2-aminopurine riboside (range from 10.4 to 11.8 ns) (*36*). This is because the time window of the femtosecond experiment is too short to reliably determine this slowest decay component. The specific choice of the fixed values for this component on the order of 10−11 ns does not affect the fitting of the first three ultrafast components, but our testing indicated that the fitting does not converge if it is not fixed. The third component, typically on the order of hundreds of picoseconds, need not be fixed because it can still be sufficiently determined.

For anisotropy decay, separate fluorescence upconversion transients were first collected for the emission polarization parallel or perpendicular to the excitation. To account for possible excitation power fluctuation between the two measurements, the fluorescence intensities for a solution of free 2-aminopurine base were measured at two time delay points of −10 and 400 ps following each transient acquisition of the RNA constructs. The fluorescence intensity of 2-aminopurine at −10 ps delay is used as background. At a time delay of 400 ps, the anisotropy decay of free 2-aminopurine base is complete, and identical intensity should be observed between parallel and perpendicular polarization. The differences in intensity between these two time delays of −10 and 400 ps for either parallel polarization or perpendicular polarization were used to calibrate the two polarization transients of RNA constructs. Femtosecond time-resolved anisotropy, $r(t)$, was constructed using the equation (*37*):

$$r(t) = \frac{I_{||}(t) - I_{\perp}(t)}{I_{||}(t) + 2I_{\perp}(t)} \quad (1)$$

where $I_{||}(t)$ and $I_{\perp}(t)$ are the calibrated fluorescence transients with emission polarization parallel and perpendicular to the excitation polarization, respectively. The time-resolved anisotropy $r(t)$ was then fitted with a multiple exponential function with one to three terms.

RESULTS

Design of RNA Duplex Constructs with 2-Aminopurine as the Dangling End Base. The fluorescence purine base analogue 2-aminopurine (Figure 1A) is a popular probe for studying nucleic acid structures and dynamics and nucleic acid−protein interactions. Previously, it has been shown that ultrafast charge transfer reaction between the excited state of 2-aminopurine and stacked nucleobases is the main channel of fluorescence quenching (*35, 38–40*). All natural bases can act as quenchers, each with unique ultrafast quenching dynamics within the picosecond (ps) to nanosecond (ns) time regime that can be resolved by ultrafast fluorescence spectroscopy with femtosecond time resolution. For example, relevant to the present investigation, G, C, and A bases quench 2-aminopurine on 3−20, ~40, and 80−200 ps time scales, respectively (*35, 40*). Efficient quenching via charge transfer requires that the quencher bases are stacked with 2-aminopurine; thus capturing the ultrafast charge transfer dynamics can provide direct information on the stacking interactions involving the fluorescent probe and the quencher bases (*33, 41, 42*). Our recently developed femtosecond dynamics approach for probing detailed RNA conformational distributions focuses on capturing the complex quenching dynamics of 2-aminopurine incorporated in

[1] Abbreviations: P, 2-aminopurine; Z, 7-deazaguanine; R, purine (A or G); fwhm, full width at half-maximum; OPA, optical parametric amplifier.

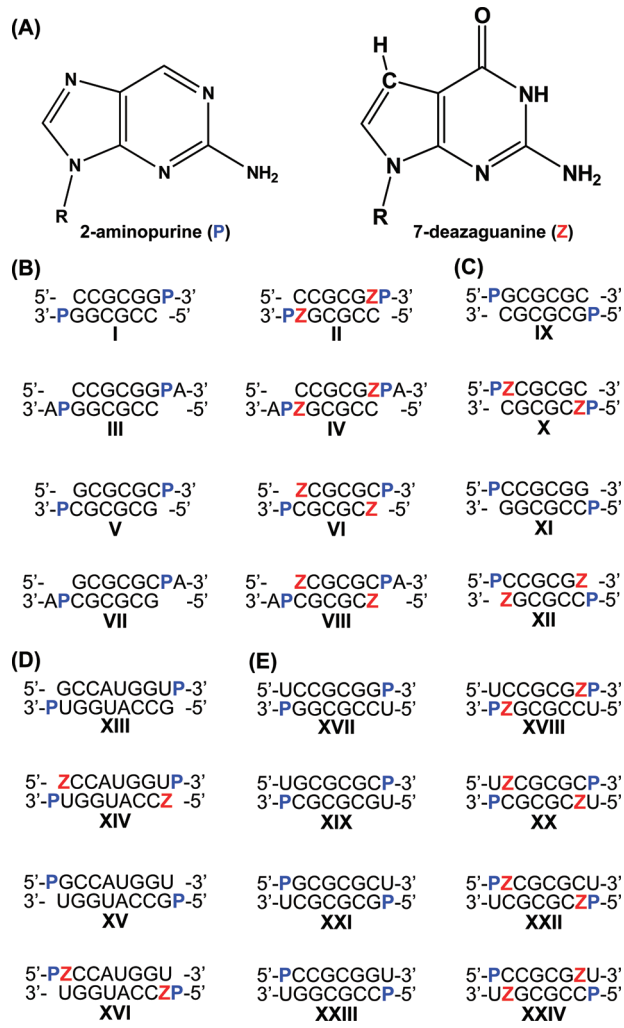

FIGURE 1: Model RNA duplex systems used in this study. (A) The chemical structures of 2-aminopurine (P) and 7-deazaguanine (Z). Designed RNA duplex constructs with (B) 3′-P or 3′-PA dangling ends on GC or ZC pairs (I−VIII), (C) 5′-P dangling ends on GC or ZC pairs (IX−XII), (D) dangling P on UG pair (XIII−XVI), and (E) PU terminal pair (XVII−XXIV). The modified bases P and Z are colored blue and red, respectively, in the sequences.

specifically designed constructs (*33*). Typically, the fluorescence decay for 2-aminopurine incorporated in nucleic acids is multiphasic in the picosecond to nanosecond time regime, characteristic of multiple coexisting conformations. The number of such distinct picosecond components and their relative amplitudes within a single decay profile relate to the minimal number of conformational substates with different stacking patterns between the probe and the quencher bases and their relative abundance in the conformational ensemble. This allows us to map the heterogeneous base stacking patterns, thus revealing unique structural features that are not easily resolved by other methods due to fast interconversion.

To probe the nature of the stacking structures and the dynamics of dangling ends, we designed a series of RNA duplex constructs with 2-aminopurine (denoted as P in the sequences thereafter) as either a single 5′- or 3′-dangling base or PA as a 3′-dangling doublet (Figure 1B−D). Probing the ultrafast fluorescence decay dynamics of P as a dangling end base allows us to monitor the stacking interactions between P and the terminal pairs, especially the heterogeneous nature of such interaction modes. In some of the constructs, the guanine base in the terminal GC pairs was also replaced by 7-deazaguanine (Z, Figure 1A). The modified base Z quenches P fluorescence on the ∼1 ps time scale, a unique rate that is faster than those observed for all natural bases (*40*). On the ∼1 ps time scale, relevant RNA structures are mostly static; the dynamic structural equilibrium is frozen on such ultrafast charge transfer time scale. We recently demonstrated that incorporation of such a modified base can provide unambiguous site-specific information regarding the nature of stacking interactions in RNA motifs and thus facilitated assignments of specific interactions (*33*), without complications from other dynamic processes that may act to gate the charge transfer reaction (*39*). The amplitudes of the picosecond components within a decay profile provide quantitative information on the relative populations of the RNA where the dangling end P base is stacked with the terminal base pair. The remaining slow decay components represent other conformations where P is not stacked. Therefore, the stacked versus unstacked populations can be quantitatively resolved. We have also designed constructs where the P base, either as a 5′-dangling end or a 3′-dangling end, can potentially form a base pair with a uridine base on the opposite strand (Figure 1E). We are interested in whether such base pairing interactions through hydrogen bonds may influence or alter the stacking interactions of the dangling end purine base and its associated dynamics in a context-dependent manner.

Thermodynamic Contributions of 2-Aminopurine as the Dangling End Base. We first examined whether 2-aminopurine as dangling end bases provides stabilization to the core RNA duplexes to the similar extent as observed previously for the natural purine bases. UV optical melting performed on these constructs (Table S1 of Supporting Information) allowed us to assess such stability contributions. Since all of our femtosecond time-resolved fluorescence experiments are performed in much lower ionic strength than typically used for RNA thermodynamics measurements (1 M NaCl), we measured these stability enhancements in 100 mM NaCl but also tested some constructs in 1 M NaCl for direct comparisons as well (Table S1 of Supporting Information). Table 1 presents the thermodynamic parameters of stability enhancement per dangling end in different contexts calculated within the framework of the nearest-neighbor model (*9*). These stability enhancements are similar in trend to the effects of a dangling purine base in otherwise identical contexts measured in high salt (*6, 10–13*). Generally, as expected, a 3′-P is much more stabilizing than a 5′-P, and the effect of 3′-P is strongly dependent on the orientation of the terminal GC base pairs (Table 1). For example, a 3′-P on a CG pair, in the context of $^{CP3'}_{G}$, provides 1.4 kcal/mol stabilization in $\Delta\Delta G^{\circ}_{37}$, compared to 0.9 kcal/mol if the orientation of the CG is switched to GC in $^{GP3'}_{C}$; both are similar in trend to the values of 1.7 kcal/mol and 1.1−1.3 kcal/mol observed for 3′-A or 3′-G in the respective contexts measured in high salt (*7*). In the case of $^{CP3'}_{G}$, both the core duplex and the duplex with the 3′-P are more stable in 1 M NaCl (Table S1 of Supporting Information), but the contribution by the dangling end is not sensitive to the total salt concentration (1.4 kcal/mol under both high and low salt, Table 1). The small difference between a 3′-P (1.4 kcal/mol) and a 3′-A (1.7 kcal/mol) may be due to the difference in the dipole moments between 2-aminopurine and adenine (6-

Table 1: Thermodynamic Stabilization of RNA Duplexes by 3′- and 5′-Dangling P and Terminal PU Pairs

dangling ends	$\Delta\Delta G^\circ_{37}$ (kcal/mol)[a]	$\Delta\Delta H^\circ$ (kcal/mol)[a]	$\Delta\Delta S^\circ$ [cal/(mol·K)][a]	dangling ends	$\Delta\Delta G^\circ_{37}$ (kcal/mol)[a]	$\Delta\Delta H^\circ$ (kcal/mol)[a]	$\Delta\Delta S^\circ$ [cal/(mol·K)][a]
			3′-P on Terminal GC Pair				
$^{GP3'}_{C}$	−0.9	−2.3	−5.0	$^{GPA3'}_{C}$	−1.1	−4.8	−11.8
$^{ZP3'}_{C}$	−0.4	−0.2	0.9	$^{ZPA3'}_{C}$	−0.8	−3.0	−7.1
$^{CP3'}_{G}$	−1.4 (−1.4)[b]	−3.8 (−3.9)[b]	−7.9 (−8.2)[b]	$^{CPA3'}_{G}$	−1.8	−7.2	−17.5
$^{CP3'}_{Z}$	−1.0	−4.8	−12.3	$^{CPA3'}_{Z}$	−1.5	−6.4	−15.8
			5′-P on Terminal GC Pair				
$^{5'PG}_{C}$	0.1	1.2	3.5	$^{5'PC}_{G}$	−0.1	−0.6	−1.5
$^{5'PZ}_{C}$	0.0	0.9	3.1	$^{5'PC}_{Z}$	0.0	0.4	1.7
			Dangling P on Terminal UG Pair				
$^{UP3'}_{G}$	−0.9	−3.9	−9.7	$^{5'PG}_{U}$	0.5	2.8	7.8
$^{UP3'}_{Z}$	−0.7	−3.7	−9.9	$^{5'PZ}_{U}$	0.4	1.8	4.3
			Terminal PU Pair				
$^{GP3'}_{CU}$	−1.1	−2.5	−4.5	$^{5'PG}_{UC}$	−1.1	−4.1	−9.6
$^{ZP3'}_{CU}$	−0.5	1.4	6.3	$^{5'PZ}_{UC}$	−0.9	−1.4	−1.8
$^{CP3'}_{GU}$	−1.1	−2.1	−3.3	$^{5'PC}_{UG}$	−1.3	−4.6	−10.9
$^{CP3'}_{ZU}$	−0.9	−1.3	−1.4	$^{5'PC}_{UZ}$	−0.7	−0.5	0.8

[a] Calculated as half of the difference in free energy changes at 37 °C (ΔG°_{37}), ΔH°, and ΔS°, respectively, between duplexes with the dangling ends (or terminal PU pair) and corresponding core duplexes, measured in 100 mM NaCl, 20 mM phosphate, 0.2 mM EDTA, and pH 6.5 (Table S1 of Supporting Information). Uncertainties in $\Delta\Delta G^\circ_{37}$, $\Delta\Delta H^\circ$, and $\Delta\Delta S^\circ$ are 0.1−0.2 kcal/mol, 1−2 kcal/mol, and ∼5 cal/(mol·K), respectively. [b] Measured in 1 M NaCl, 20 mM sodium cacodylate, 0.5 mM EDTA, and pH 7.0.

aminopurine). An extra adenine base that is 3′ to the dangling P (i.e., $^{CPA3'}_{G}$) provides only small additional (0.2−0.5 kcal/mol) stability compared to a single 3′-P (Table 1), consistent with earlier reports on the marginal effects by extra dangling adenine bases (*25, 27*). For P as the 5′-dangling end base, as expected, there is little contribution to the stability of the core duplex within experimental uncertainty for such measurements. It appears that the contribution by a dangling P is slightly less for constructs with ZC as terminal base pairs compared to GC pairs (Table 1). A recent study of the effects of Z modification on DNA stability suggested that such modification, although not affecting the stacking structural geometry and hydrogen-bonding interactions compared to a natural G base, may possibly interfere with cation binding and hydration involving the N7 of guanine and affect the strength of the neighboring base pair, but both stabilization and destabilization effects have been observed in different contexts (*43*).

Thermodynamic effects of dangling ends on duplexes that end with non-Watson−Crick pairs, e.g., UG or GA pairs, although known to frequently occur in RNA (*15*), have not been examined systematically. One limited study reported a 1.0 kcal/mol contribution by a 3′-A in the context of $^{UA3'}_{G}$ (*44*), an effect that is seemingly between those of the dangling purine base on Watson−Crick CG (1.7 kcal/mol) and UA pairs (0.7 kcal/mol) (*7*). For P as a dangling end 3′ to the base U of a terminal UG (or UZ) pair, in the context of $^{UP3'}_{G}$ (or $^{UP3'}_{Z}$), it contributes 0.9 kcal/mol (or 0.7 kcal/mol), similar to the 1.0 kcal/mol stabilization by an adenine base in such context in high salt (*44*). For P as a dangling end base that is 5′ to the G (or Z) of the GU (or ZU) pair, it contributes no stabilization to the core duplexes, similar to the lack of stabilization by a 5′-P on the terminal GC pair as discussed above.

If a uracil base is incorporated on the opposite strand from the dangling P, the two bases can potentially form a PU pair similar to the Watson−Crick AU pair. There are two orientations for the PU pair relative to the terminal GC pair. When a 3′-P pairs with a 5′-U to form a terminal PU pair adjacent to GC pair, the potential new hydrogen-bonding interactions provide little added stability compared to the stabilizing effects of a single 3′-P, regardless of the orientation of the GC pair (Table 1). This is also consistent with the lack of stabilization by a 5′-dangling U base (*7*). However, in the cases where a 5′-P pairs with a 3′-U, the duplexes with the PU pair are about 0.7−1.3 kcal/mol more stable per PU pair than the duplexes with only 5′-P as dangling bases (Table 1). A significant portion of the stabilization in these cases is likely contributed by the added U as a 3′-dangling base on a CG or GC pair. Such contribution can be 0.6−1.2 kcal/mol in high salt, depending on the orientation of the GC pair (*7*). These observations are similar to those for corresponding duplexes of natural sequences (*8*). This raises the question regarding the interplay between the two favorable interactions, i.e., base stacking of the two individual dangling bases and the hydrogen-bonding interactions between the two bases, which need to be optimized to stabilize the RNA structures in a given context.

The thermodynamic parameters of $\Delta\Delta H^\circ$ and $\Delta\Delta S^\circ$ are similarly calculated (Table 1). Although these parameters are not as reliable as $\Delta\Delta G^\circ$ values (*8*), comparisons of their values can still be meaningful. Comparisons of these values for dangling ends on both GC and GU pairs revealed that, in general, more negative values of $\Delta\Delta H^\circ$ and $\Delta\Delta S^\circ$ are observed for 3′-dangling ends than for 5′-dangling ends. This is consistent with a picture where there are more favorable interactions involving a 3′-dangling base than a 5′-dangling base, with enthalpy being the driving force (*6, 10*). Formation of a base pair with U tends to make $\Delta\Delta H^\circ$ and $\Delta\Delta S^\circ$ more negative for constructs with a 5′-dangling P base, suggesting that more favorable interactions result and such interactions lower its conformational freedom. For the constructs with 3′-dangling ends, however, the effects of PU pair formation are much smaller, the energetics of the 3′-dangling P dominates, and there is no significant change in the interactions involving the 3′-P base.

Table 2: Parameters of Femtosecond Time-Resolved Decays for RNA Constructs[a]

construct	dangling end	τ_1 (ps)	A_1 (%)	τ_2 (ps)	A_2 (%)	τ_3 (ps)	A_3 (%)	τ_4[b] (ps)	A_4 (%)
				3′-P or 3′-PA on GC Pair					
I	$^{GP3'}_{C}$	3.7	32	12	50	92	9	11300	9
II	$^{ZP3'}_{C}$	1.1	70	14	8	261	5	11300	17
III	$^{GPA3'}_{C}$	6.5	35	23	49	182	8	11300	8
IV	$^{ZPA3'}_{C}$	1.2	62	10	12	171	11	11300	15
V	$^{CP3'}_{G}$	3.2	55	19	19	174	18	11300	8
VI	$^{CP3'}_{Z}$	1.2	56	10	19	89	15	11300	10
VII	$^{CPA3'}_{G}$	4.0	49	15	28	202	15	11300	8
VIII	$^{CPA3'}_{Z}$	1.4	53	13	20	129	16	11300	11
				5′-P on GC Pair					
IX	$^{5'PG}_{C}$	4.5	32	34	20	321	14	11300	34
X	$^{5'PZ}_{C}$	2.1	35	19	15	292	20	11300	30
XI	$^{5'PC}_{G}$			48	28	176	54	11300	18
XII	$^{5'PC}_{Z}$			12	13	110	69	11300	18
				Dangling P on UG Pair					
XIII	$^{UP3'}_{G}$	5.5	48	18	31	97	8	11300	13
XIV	$^{UP3'}_{Z}$	1.5	46	12	24	99	10	11300	20
XV	$^{5'PG}_{U}$	6.6	33	35	24	391	15	11300	28
XVI	$^{5'PZ}_{U}$	1.2	47	14	16	127	16	11300	21
				Terminal PU Pair					
XVII	$^{GP3'}_{CU}$	3.3	57	12	32	155	4	11300	7
XVIII	$^{ZP3'}_{CU}$	0.9	76	7	8	119	5	11300	11
XIX	$^{CP3'}_{GU}$	3.0	54	12	21	117	16	11300	9
XX	$^{CP3'}_{ZU}$	1.2	53	10	21	85	14	11300	12
XXI	$^{5'PG}_{UC}$	1.8	71	35	11			11300	18
XXII	$^{5'PZ}_{UC}$	0.8	58	15	11	388	12	11300	19
XXIII	$^{5'PC}_{UG}$					108	92	11300	8
XXIV	$^{5'PC}_{UZ}$			17	32	64	58	11300	10

[a] Decay lifetimes and amplitudes for each construct are represented by τ (ps) and A (%), respectively. Estimated errors are within 5%. [b] Parameter τ_4 is fixed at the average of the observed lifetime of free 2-aminopurine (11.3 ns) (*36*), because the time window of the femtosecond experiment is too short to reliably determine the slowest decay component (see Experimental Procedures).

These observed thermodynamic effects by the dangling P base on the core RNA duplexes suggest that the P base behaves similarly to the natural purine bases as dangling ends, particularly in terms of the stacking interactions between the dangling base and the terminal base pairs. This allows us to use it as a probe to exam the dynamic behavior of dangling purine bases and provide a dynamic structural basis for the differential thermodynamic stability enhancement by the dangling end bases in different contexts.

3′-Dangling Ends Feature a High Stacked Subpopulation That Depends on the Orientation of the Terminal GC Pair. As observed in other DNA and RNA constructs with internally incorporated 2-aminopurine as the structural probe, the femtosecond time-resolved fluorescence decay for our dangling end constructs displays multiexponential decay dynamics in the picosecond to nanosecond time regime under magic angle condition. The resolved decay components reflect the conformational heterogeneity of the probe as a dangling end base in its various contexts. The characteristic decay time scales provide information on the nature of the base−base stacking interactions, and the amplitudes associated with these decay components reflect the relative populations of the conformational distributions. Table 2 lists the decay dynamic parameters for all constructs. Figure 2 shows the decay profiles for constructs with 3′-P on GC (I) or ZC (II) (Figure 2A), 3′-P on CZ (VI, Figure 2B), and 5′-P on ZC (X, Figure 2C) and CZ (XII, Figure 2D). Decay profiles for corresponding constructs with 5′- or 3′-P on GC or CG pairs are presented in Supporting Information. Constructs I ($^{GP3'}_{C}$) and V ($^{CP3'}_{G}$) with a 3′-P on the GC or CG

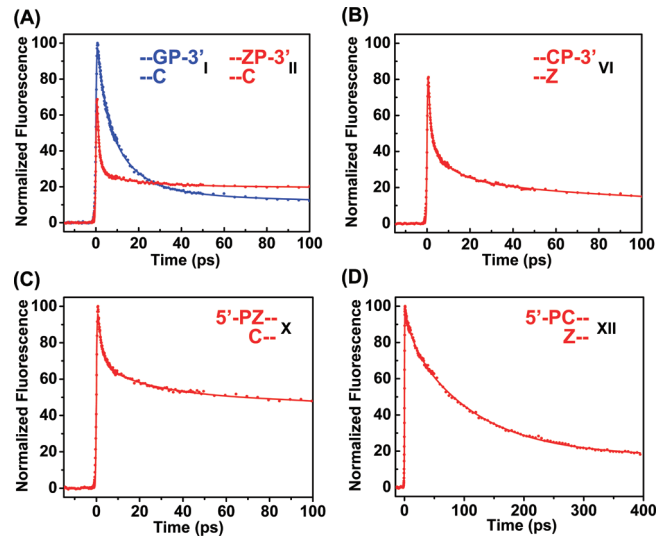

FIGURE 2: Normalized femtosecond time-resolved fluorescence decay profiles (magic angle) for RNA duplexes with single dangling end base. Decays are shown for constructs with 3′-P on (A) terminal GC pair (I, blue) and ZC pair (II, red) and (B) terminal CZ pair (VI) and constructs with 5′-P on (C) terminal ZC pair (X) and (D) terminal CZ pair (XII). Profiles are normalized to the longest nanosecond component, rather than the initial intensity because the fast decay components (~1 ps) for constructs II and VI are too close to the cross-correlation of the laser pulses; therefore, significant decay occurs during the excitation pulse.

pair exhibit primary decays (the fastest components) of 3−4 ps (Table 2), consistent with stacking of P on a guanine base (*35, 40*). These results hint that a 3′-P can interact with

the G base in the terminal GC pair via either intrastrand (I) or cross-strand (V) stacking modes, depending on the orientation of the GC base pairs. Potential quenching reaction by the C base in these constructs would produce decay rates that are much slower (~40 ps) (*35, 40*), thereby not interfering with the interpretation. As we have demonstrated recently (*33*), more definitive and unambiguous information on specific base−base stacking interactions can be revealed and confirmed from the constructs containing Z modifications, in comparison with the constructs without such modifications. For constructs II ($^{ZP3'}_{C}$) and VI ($^{CP3'}_{Z}$), the fastest primary dynamics are 1.1 ps (70%) and 1.2 ps (56%), respectively (Table 2). These ultrafast dynamic components must be due to direct static base stacking interactions between the two bases P and Z in these RNAs, because there is no other mechanism that can produce such ultrafast quenching rates in these constructs (*33, 40*). The two bases of the terminal ZC pair are the only bases that P can interact with. The relative amplitudes of these ultrafast components represent the fraction of the population that P and Z bases are statically stacked on the ground state within the experimental time window, so the ultrafast excited-state quenching channel for P via charge transfer reaction with Z is available. Specifically, the large amplitude of this ultrafast decay for construct II indicates that the single 3′-P mostly stacks on the neighboring Z base of the same strand. When the orientation of the terminal pair is switched (construct VI), however, the P base mainly experiences cross-strand stacking with Z on the opposite strand instead. Therefore, these ultrafast decay dynamics unambiguously define the context-dependent purine−purine stacking interactions between the dangling base P and the Z of the terminal pairs. Apparently, the orientation of the terminal base pair determines the exact nature (interaction partner) of the stacking interactions for a major population in these contexts. As a control, when the duplex constructs II and VI are denatured by the presence of 40% formamide, the characteristic ultrafast decay components disappear (see Figure S1 of Supporting Information).

The decay profiles for constructs without Z modification (I, Figure 2A, and V, Figure S2 of Supporting Information) are consistent with this picture. The first decay components (3−4 ps) apparently are from direct static stacking interaction between the P and G base, reflecting the same type of stacking interactions between P and Z in the Z-containing constructs. The second decay components, typically on the time scale of 10−20 ps that are observed for most of the constructs (Table 2), are not due to stacking interaction between the P and base of cytosine because such stacking interaction is expected to quench fluorescence of P on the slower time scale (~40 ps) (*35*). Apparent charge transfer reaction rates on the 10−20 ps regime are often observed along with faster rates, even in short single-stranded oligomer constructs where P is adjacent to only one type of quencher base (*40*). For example, when P is placed adjacent to a single Z base (dimer oligo 5′-PZ-3′) or flanked by Z on both sides (trimer oligo 5′-ZPZ-3′), there are 10−20 ps components observed along with the ~1 ps components. Most likely, such components represent small-scale local dynamic motion of either the P base or the quencher base around the glycosidic bond. Such base dynamics have been detected by NMR spectroscopy (*45, 46*). From analysis of NMR relaxation experiments, information on the amplitudes and time scales of base motions can be derived. Base planes have been found to undergo up to about 20° of fluctuation around the glycosidic bond on a time scale of a few picoseconds to tens of picoseconds. Such internal local base dynamics on this time scale will be a rate-limiting step that can modulate the ultrafast charge transfer reaction between P and G/Z, which requires significant overlap of the two bases, through a conformation-gating mechanism (*39*). Therefore, observed apparent decay dynamics on the 10−20 ps time scale are modulated charge transfer rates due to base motions of either the P base or the quencher, or both. We consider these 10−20 ps components to also represent the "stacked" conformation, as the dynamic base motion on such time scale typically is within a small range of angles (*45, 46*). Therefore, both of the two fastest components collectively represent a subpopulation of conformations where the dangling end base P stacks on the G or Z of the terminal base pair. The amplitudes of the two components add up to 74−82% of total population for these constructs with the single 3′-dangling P (Table 2). Note that because the base dynamic motion on the 10−20 ps time scale is closer to the time scale of the static quenching rate of P by G than that by Z, the relative amplitudes of the 3−4 ps quenching components by the G base are more affected than the faster ~1 ps quenching components by Z. This explains the relatively smaller ratios of the amplitudes between the first and the second components for the constructs with the terminal GC pair than those with the ZC pair. The sums of the amplitudes of the two components are similar.

The observed decay components on the ~100−300 ps time scale of relatively low amplitudes for these constructs cannot be uniquely assigned on the basis of the fluorescence decay under magic angle condition alone, as such components can potentially represent either a direct charge transfer reaction with a statically stacked base with slow charge transfer rate (e.g., adenine base) or a dynamic conformation-gated charge transfer reaction (*39*). Anisotropy decay data discussed below suggest that there is a dominant hindered base dynamic motion for the dangling end base on a similar time scale that can act as the rate-limiting step in the charge transfer reaction with the terminal base pair (100−200 ps) and contribute to these apparent observations. There is always a decay component on the slow nanosecond time scale for all of the constructs. Note that due to our short observation time window (~400 ps), this component cannot be uniquely determined; therefore, it is fixed at the average intrinsic lifetime (11.3 ns) for the free 2-aminopurine base in solution (*36*) and should be considered to represent a combination of decays on the nanosecond time scale. This slow decay component represents the P base that behaves like a free base in solution that lacks any significant base stacking, and therefore no ultrafast quenching pathways exist for P in such conformation(s). The amplitude of this component therefore is proportional to the conformation(s) where the P base is not stacked with any other base in the structures.

An Additional Dangling Base Does Not Significantly Alter the Population Distributions of 3′-Dangling Ends. Additional bases extending the single-stranded dangling ends have been observed to provide small added stability in high salt (*25, 27*). These enhancements are rather marginal considering the uncertainty of the thermodynamic measurements using UV optical melting methods (*8*). Although relatively much

smaller, the additional stabilization is possibly due to extended intrastranded stacking between the first base and the additional dangling bases (*25*). It was proposed that the additional bases can possibly reduce the dynamics of the first dangling base and increase the dwell time in the stacked state, thereby providing more stabilization (*30*). Our thermodynamic measurements which showed a small increase in stability contributed by an extra adenine on a 3′-P base, under low salt conditions, are consistent with these earlier observations (Table 1). We wanted to examine whether an adenine base added to the 3′-side of a 3′-dangling P would influence the observed decay dynamics profiles through possible intrastrand P/A base stacking (*30*). Comparisons for decay profiles between constructs I and III, II and IV, V and VII, and VI and VIII (Figure S2 of Supporting Information) indicate that such an extra adenine base does not significantly change the decay profiles, in terms of both the decay rates and associated amplitudes (Table 2). Therefore, an extra adenine base does not further enhance the stacking interactions between a 3′-P and the terminal pair and does not alter the associated population distributions for a 3′-P significantly.

Taken together, the presence of these multiple decay components, which is characteristic of different stacking interactions or lack of them, points to a picture of a conformational ensemble for a purine base as the 3′-dangling end. A 3′-dangling purine base dynamically samples a number of substates, dominated by a high subpopulation of a conformation where it stacks on the terminal GC pair. For either single dangling P or double dangling PA, the total population of 3′-P stacked on the terminal base pair is 73−84%, reflected in the sum of the relative amplitudes of the two fastest decay components for these constructs (Table 2). As discussed above, these ultrafast decay components captured either the direct static stacking interactions or stacking that is slightly modulated by small range base dynamics. The nature of the stacking interactions is dependent on the relative orientations of the terminal GC base pair. In the context of $^{GR3'}_{C}$, where R is the dangling purine base, the 3′-purine mostly stacks on the adjacent 5′-G of the same strand, while in the context of $^{CR3'}_{G}$, the 3′-purine mostly stacks on the G of the opposite strand. Obviously, these stacked conformations are not static structures but are at equilibrium with a low population of unstacked conformation(s), which also implies stacking/unstacking conformational dynamics on certain time scales. The relative dwell times of the dangling base in these different structures produce the equilibrium picture of an ensemble of stacked (intrastrand and cross-stranded) and unstacked conformations, and this equilibrium apparently is correlated with the thermodynamic stability enhancements. The higher cross-stranded stacking population leads to the more significant stabilization.

5′-Dangling Ends Have a Lower Subpopulation of Stacking with the Terminal Base Pair. Figure 2 also shows the decay profiles for constructs with 5′-P on the ZC pair (X) and the CZ pair (XII). In marked contrast to the 3′-dangling P cases, there is no ∼1 ps dynamic component (Table 2) observed for these constructs. Constructs IX ($^{5'PG}_{C}$, Figure S4) and X ($^{5'PZ}_{C}$, Figure 2C) have a 4.5 ps and a 2.1 ps component, respectively, of similar amplitudes (32% and 35%). These components represent the static stacking of 5′-P on the G or Z purine bases of the same strand. The fact that the 2.1 ps component for construct X is slower than the ∼1 ps components observed for 3′-dangling P constructs indicates that the intrastranded 5′-P/Z (or 5′-P/G) stacking may feature only partial base overlap. The total amplitudes of the first two components for these 5′-P constructs (∼50%) are lower than those for the 3′-P cases. Correspondingly, the amplitudes of the nanosecond components (34% and 30%) are also relatively larger. For constructs XI ($^{5'PC}_{G}$) and XII ($^{5'PC}_{Z}$, Figure 2D), there is very little cross-strand purine−purine stacking, in marked contrast to the observations for 3′-P. The dominant decay components for these two constructs are in fact on 176 and 110 ps time scales (54% and 69%), which may represent charge transfer that is gated by some type of hindered conformational dynamics of the bases (*39*), as suggested by anisotropy decay discussed below.

Dangling Ends on the Terminal UG Pair. Our thermodynamic measurements of P as a 3′-dangling end base on a UG pair (Table 1) suggested that a dangling P provides 0.9 and 0.7 kcal/mol stability to duplexes with a terminal UG and UZ pair, respectively, similar to previously observed 1.0 kcal/mol in high salt for an adenine as the dangling end base on the UG pair (*44*). As a 5′-dangling end, however, P does not provide any stabilization, similar to a 5′-dangling base on a Watson−Crick pair. The dynamic decays of P as either a 3′- or a 5′-dangling base in constructs with terminal UG or UZ base pairs (XIII−XVI) are shown in Figure S3 of Supporting Information. Apparently, a 3′-P on the UG or UZ pair (constructs XIII, $^{UP3'}_{G}$, and XIV, $^{UP3'}_{Z}$) has a significant population of cross-strand stacking with the G/Z purine base on the opposite strand (46−48% for the fastest component, 5.5 ps for XIII and 1.5 ps for XIV; 31% and 24% for the second component, 18 and 12 ps, respectively). This gives about 70−80% total amplitudes of the first two components, similar to a 3′-P on the CG pair (Table 2). As a 5′-P on the GU pair, construct XV ($^{5'PG}_{U}$) has a very similar decay profile as that of construct IX ($^{5'PG}_{C}$) with a 5′-P on a GC pair, in terms of both decay time scales and amplitudes, suggesting that both have a similarly low population of intrastranded stacking with the G base. For construct XVI ($^{5'PZ}_{U}$) with a 5′-P on a ZU pair, however, the observed 1.2 ps primary decay component (47%) is faster than the 2.1 ps observed for a 5′-P on a ZC pair in construct X ($^{5'PZ}_{C}$), and this construct also has somewhat higher amplitude of this ultrafast component.

Anisotropy Decays Reveal Base Motions of Dangling Ends. Conformational dynamics of nucleic acids can span a wide range of time scale and length scale (*32*). On the basis of our femtosecond time-resolved fluorescence decays of the P base as dangling ends discussed above, which were measured under magic angle condition, it is apparent that a dangling end P samples multiple conformations. The multiple conformations are manifested in the multiple dynamic time scales within the decay profiles. Presumably, the dangling end base can undergo stacking/unstacking dynamics resulting in a certain population distribution between the stacked and unstacked states. It has been proposed that a 5′-phosphate restricts the conformation of the sugar and base of a 5′-dangling nucleotide (*6, 11*), while on the basis of early observations on the NMR scalar coupling constants of ribose protons for dangling bases, a 3′-dangling purine retains some flexibility when stacked at the end of a duplex (*5*).

In order to probe the mobility of the 5′- and 3′-dangling bases, we performed femotosecond time-resolved anisotropy

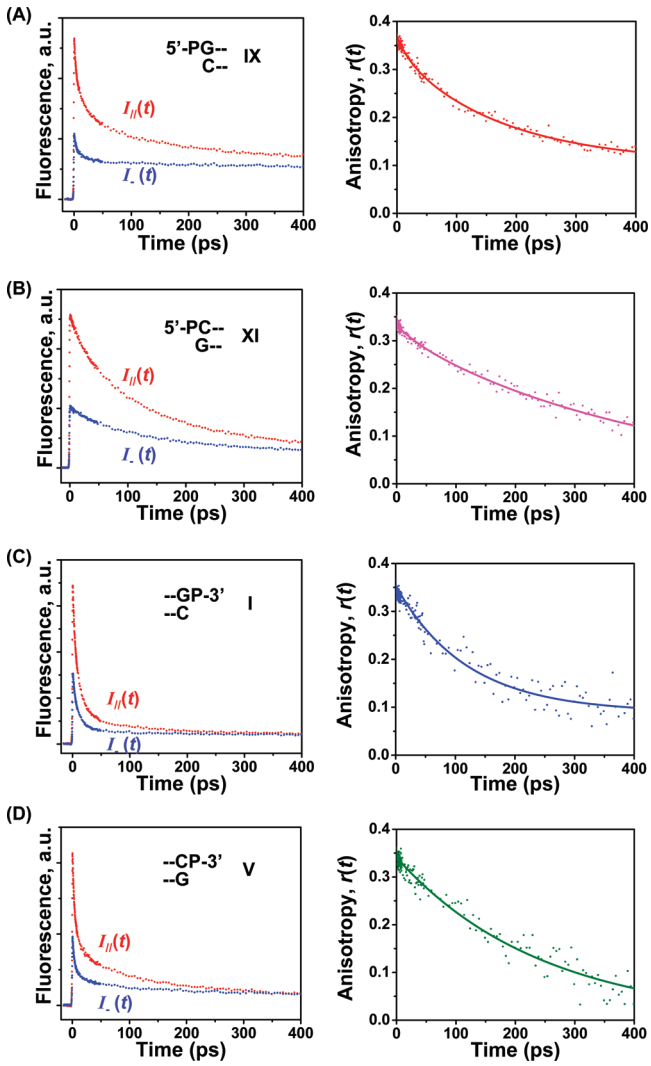

FIGURE 3: Femtosecond time-resolved anisotropy decays for constructs with 5′-dangling end (A) construct IX and (B) construct XI and 3′-dangling end (C) construct I and (D) construct V. Left panels: Fluorescence decay profiles measured with parallel ($I_{||}$, red) and perpendicular ($I_{\perp}$, blue) polarization to that of the excitation. Right panels: Anisotropy decay, $r(t)$, constructed from $I_{||}$ and $I_{\perp}$. Solid lines are the best fits.

decays of P using constructs I ($^{GP3'}_{C}$), V ($^{CP3'}_{G}$), IX ($^{5'PG}_{C}$), and XI ($^{5'PC}_{G}$) (Figure 3). Due to significant loss of fluorescence within the ~1 ps time window, the anisotropy decay properties for constructs with Z modification were not investigated. For constructs I, V, IX, and XI, the constructed anisotropy decay profiles can be best fitted by one to three exponential terms with various time scales and amplitudes (Table 3). The measured fundamental anisotropy at time zero (r_0) with femtosecond time resolution falls within the range of 0.33−0.37, compared to the theoretical maximal value of 0.4 for an isotropic solution (*37*). Such values for the fundamental anisotropy for 2-aminopurine incorporated in nucleic acids are typical (*47*). The anisotropy decay components on the ~nanosecond time scale for some of the constructs (Table 3) are consistent with overall tumbling rotation of the entire duplex in aqueous solution (*37*). There is a 21 ps and a 40 ps anisotropy decay component for constructs IX and XI, respectively, that represents small-scale base motion of P as the 5′-dangling end on the GC pair, but such motion only makes a very small contribution to the overall anisotropy decay. The most dominant internal motion of the P base in these constructs is on the time scale of hundreds of picoseconds. Base dynamic motions on such time scales are considered to represent hindered motion of the base in the strand (*47*). Such motions can become the rate-limiting step in the charge transfer reaction and act to gate the ultrafast charge transfer between the excited-state P and the neighboring quencher base, which give rise to fluorescence decay on these similar time scales. For example, the third components of the decay profiles under magic angle condition for all RNA constructs discussed above are typically on the hundreds of picoseconds time scales (Table 2). These quenching dynamic components most likely represent the charge transfer reactions gated by the hindered base conformational dynamics on the time scales revealed in the anisotropy decay measurements. Total unstacking of bases, however, typically occurs on a longer time scale, e.g., nanoseconds to hundreds of nanoseconds (*32*), depending on the structural context and complexity of the conformational changes involved.

It appears that the overall anisotropy decay of a 5′-P is slower than a 3′-P, as the time-dependent fluorescence intensities of the parallel and perpendicular polarizations merge to identical values within 250−300 ps for 3′-P but are clearly still different at 400 ps for 5′-P, suggesting that a 5′-P base is somewhat more rigid overall. This is consistent with the earlier proposal that a phosphate 5′ to the end of the duplex can restrict the 5′-dangling base in an unstacked conformation (*6, 11*) and that a 3′-dangling purine retains somewhat more flexibility (*5*), which can allow it to more efficiently maximize the stacking interactions with the terminal base pair by seeking the larger guanine base as the stacking partner.

Hydrogen Bond Formation Has Different Effects on the Conformational Distribution of 5′- and 3′-Dangling P Bases. As shown in Table 1, formation of potential hydrogen bonds between the P base and a U base at the end of a core duplex has very different effects on the thermodynamic stability of the duplex depending on the orientation of the potential PU pair with respect to the adjacent GC pair. The question that remains is whether formation of such a potential PU pair through hydrogen-bonding interactions may alter the stacking interactions between the dangling base P and the terminal pair in a context-dependent manner that correlate with these thermodynamic observations.

For the cases of duplexes with 3′-P, the addition of a 5′-U contributes little added stability to the duplexes (Table 1). The ultrafast decay dynamics for such constructs with Z modifications, XVIII ($^{ZP3'}_{CU}$) and XX ($^{CP3'}_{ZU}$), are shown in panels A and B of Figure 4. These two decay profiles with 3′-P in the PU pair are very similar to those for their single dangling P counterparts, II ($^{ZP3'}_{C}$) and VI ($^{CP3'}_{Z}$), respectively. Similar comparisons can be made between decay profiles for constructs without Z modifications (Figure S4 of Supporting Information). Both the specific time scale and the amplitudes of fluorescence quenching dynamic components are similar between the two sets of constructs, with or without the 5′-U base. This indicates that the patterns of stacking interactions between the 3′-P base and the terminal GC/ZC pair, in terms of both the physical interactions (stacking geometry) and their relative population distributions, are not significantly altered by the added 5′-U base in these contexts. Therefore, both bases behave either as separate dangling end bases with no

Table 3: Parameters of Femtosecond Time-Resolved Anisotropy Decay[a]

construct	dangling end	τ_1 (ps)	r_1	τ_2 (ps)	r_2	τ_3	r_3	r_0[b]
I	$^{GP3'}_{C}$			117	0.260	~ns	0.094	0.354
V	$^{CP3'}_{G}$			245	0.341			0.341
IX	$^{5'PG}_{C}$	21	0.034	169	0.221	~ns	0.113	0.368
XI	$^{5'PC}_{G}$	40	0.021	427	0.311			0.332

[a] Anisotropy decay profiles are fitted to one to three exponential terms, each with a decay lifetime (τ_1 to τ_3) and associated amplitude (r_1 to r_3). τ_3 should be considered as an estimate of decay on the nanosecond (ns) time scale, due to the limited experimental time window. Estimated errors are within 10%. [b] The fundamental anisotropy at time zero r_0 is calculated as $r_0 = r_1 + r_2 + r_3$.

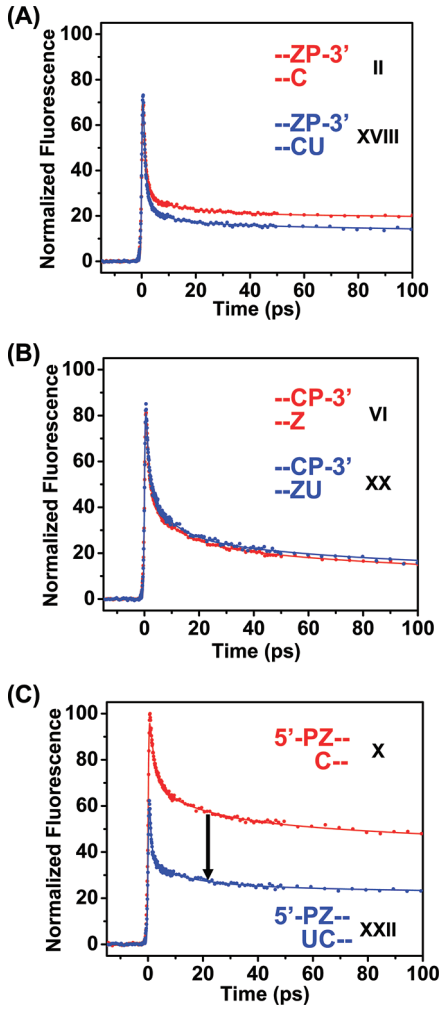

FIGURE 4: Effects of PU base pair formation on the magic angle femtosecond time-resolved fluorescence decay profiles of the dangling base P. Comparisons are shown (A) between constructs with 3′-P (II, red) and 3′-PU pair (XVIII, blue) on ZC pair, (B) between constructs with 3′-P (VI, red) and 3′-PU pair (XX, blue) on CZ pair, and (C) between constructs with 5′-P (X, red) and 5′-PU (XXII, blue) on ZC pair. The vertical downward arrow in (C) indicates the significantly larger amplitude of the ultrafast decay component for construct XXII compared to that of X. Profiles are normalized to the slowest nanosecond components, rather than the initial intensity because the fast decay components (~1 ps) for most of these constructs are too close to the cross-correlation of the laser pulses; therefore, significant decay occurs during the excitation pulse.

strong hydrogen bonds formed between them or the formation of hydrogen bonds does not alter the stacking structure involving the 3′-P base, particularly the relative position of the 3′-dangling P with respect to the terminal GC pair. This is presumably due to the strong favorable stacking interactions between the 3′-P and the G base of the terminal pair, which creates a high barrier if the stacking structures are to be altered. Consistent with this picture, a 5′-dangling U does not contribute to the duplex stability significantly (*7*).

For the cases of duplexes with 5′-P, the addition of a 3′-U significantly stabilizes the corresponding duplexes (Table 1). Comparison between the decay profile for construct XXII ($^{5'PZ}_{UC}$) to that of X ($^{5'PZ}_{C}$) shows a significantly enhanced stacked population for the 5′-P base on the ZC terminal pair, manifested by the much larger amplitude of the ultrafast decay components (Figure 4C, Table 2). Similar comparison can be made between constructs XXI ($^{5'PG}_{UC}$) and IX ($^{5'PG}_{C}$) (Figure S4 of Supporting Information). The formation of the PU pair enhanced the 2.1 ps component of 35% for construct X to 0.8 ps of 58% for XXII and, similarly, increased the 4.5 ps component of 32% for IX to 1.8 ps of 71% for construct XXI. The 11.3 ns components are also reduced from 30−34% to 18−19%. Apparently, a PU pair is formed through hydrogen-bonding interactions and thus restricts the 5′-P base in a position that is more overlapped with the adjacent G/Z base of the same strand, promoting more efficient charge transfer reaction. The unstacked population is significantly reduced as a result. Presumably, the 3′-U is stacked on the C of the GC pair, as specific electrostatic interactions between the O4 of the 3′-U and the amino group of C are the major contributor of the stabilization in these contexts (*15*). This type of interaction between specific functional groups, however, cannot be directly probed by the time-resolved spectroscopic approach here. Interestingly, the faster rates of the first components for constructs XXI (1.8 ps) and XXII (0.8 ps) compared to those for IX (4.5 ps) and X (2.1 ps) are suggestive of differences in the exact nature of the stacking interactions between a single 5′-P and a 5′-P in the PU pair with the GC or ZC pair. Changes in the time scales of decay dynamics are indicative of different stacking geometries, e.g., base overlap and relative orientations. This is in mark contrast to the cases of 3′-P discussed above, where the decay time scales are not altered by potential formation of the PU pair. The primary decay rate of 0.8 ps (1.8 ps) for 5′-P on a ZC (GC) pair is somewhat faster than the corresponding rate for 3′-P of 0.9−1.2 ps (3−7 ps). More efficient charge transfer has been observed for DNA if the P is on the 5′-side of a quencher base than if P is on the 3′-side (*48*) as in the case here. It is not clear if this trend holds for RNA in general.

For constructs XXIII ($^{5'PC}_{UG}$) and XXIV ($^{5'PC}_{UZ}$) (Figure S4), where a PU pair can be potentially formed next to the CG or CZ pair, the 11.3 ns components have somewhat smaller amplitudes (8−10%) than those for XI ($^{5'PC}_{G}$) and XII ($^{5'PC}_{Z}$) (18%), which indicates an overall slightly lower population of totally unstacked conformations for the 5′-P. However, as for XI and XII, a single component dominates the decay for these constructs, e.g., the 108 ps (92%) component for XXIII. Such observation cannot be accounted for by a static

stacking interaction between P and any base in that context and is suggestive of certain conformational dynamics on this time scale. Apparently, there is little direct cross-strand purine−purine stacking involving a 5′-P in the potentially PU-paired contexts, and the intrastrand P/C stacking is also not significant, indicating that the 5′-P is not further restricted by the 3′-U base into a PU pair. The enhanced stability measured thermodynamically is mostly due to the presence of the U as a 3′-dangling base (*7*).

DISCUSSION

RNA structures are known to be very dynamic, and they typically adopt multiple conformations under various biologically relevant conditions (*49*). RNA's ability to undergo these conformational dynamics on various time scales results in a heterogeneity at different structural levels and plays an important role in molecular recognition and functions. Because of the favorable and additive contributions from base stacking interactions, the total free energy of folding for an RNA structure can be very large (*1*) compared to that of typical protein folding. Additionally, a large number of alternative RNA structures may also have significant stability. Base stacking and unstacking conformational dynamics allow RNAs to sample multiple conformations consisting of different stacking patterns that are separated by energetic barriers of various heights. Such motions may allow optimization of specific intermolecular interactions between RNA and its partners upon binding.

Context-dependent thermodynamic stabilization of RNA and DNA duplexes by unpaired dangling end bases have long been known, and various structural models have been proposed to rationalize these observations. Stacking interactions between the dangling base and the terminal base pair in large RNAs have been found to be correlated with the measured stabilization in small model systems (*15, 30*). These correlations, however, have only been made for the static structures, and the dynamic aspects have not been fully investigated. A related question is whether the strong stacking interactions may compete with hydrogen-bonding interactions that may require a somewhat different geometry for the bases involved. Here, we aim to reveal the dynamic structural basis for the observed correlation between stacking structures and stability enhancement by dangling end bases in RNA. By capturing the multiphasic fluorescence quenching dynamics of 2-aminopurine as the dangling end base on ultrafast time scales using femtosecond time-resolved spectroscopy, we have resolved the context-dependent heterogeneous stacking structural patterns for purine dangling ends. We provide crucial evidence on the dynamic nature of the stacking interactions between the dangling end base and the neighboring base pairs.

Figure 5 presents a dynamic structural model that incorporates findings from both thermodynamic measurements and conformational heterogeneity and dynamics measurements in order to rationalize the current and previous observations for dangling ends in various contexts. Our results support the notion that, in A-form RNA, a dangling purine base samples various interaction modes and thus is in an equilibrium of multiple conformations of stacked and unstacked substates. In the case of a 5′-dangling purine on the GC pair, the dangling base is largely unstacked, particularly when the

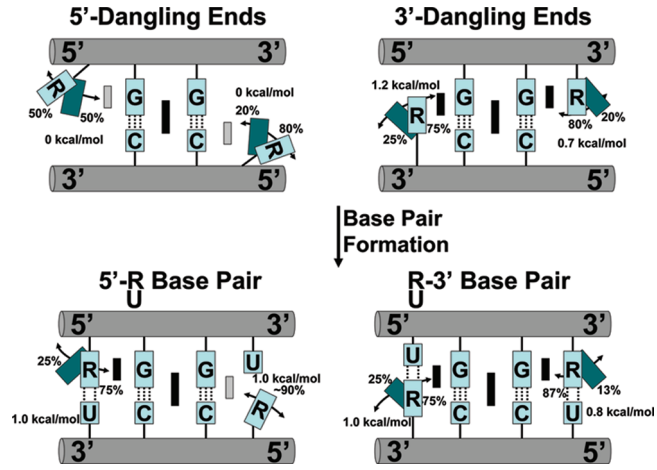

FIGURE 5: A dynamic structural model for the stacking interactions between 5′- or 3′-dangling purine (R) and terminal GC base pairs and the effects of formation of RU base pair. Gray horizontal cylinders represent RNA backbones, and the rectangles represent the bases. Curved double arrows represent stacking/unstacking dynamics of dangling bases. The positions of the dangling bases relative to the terminal base pairs in the major and minor populations (with percentages of population indicated) are represented by light blue and dark blue rectangles, respectively. The major and minor stacking interactions associated with these populations are represented by black and gray bars, respectively. Thermodynamic contributions by dangling ends or terminal RU pair (calculated as average values for relevant constructs with terminal GC and ZC pairs, Table 1) are labeled.

adjacent base that is 3′ to the dangling purine is a pyrimidine. This is consistent with the fact that a 5′-dangling base does not provide significant stabilization to the A-form RNA duplex. The anisotropy decay measurements are consistent with the hypothesis that a 5′-dangling end is relatively more rigid and is held in a largely unstacked conformation (*6, 11*). However, the unstacked conformation(s) is (are) in an equilibrium with a population that features a partial intrastranded stacking between the 5′-P and the G in the GC pair in the context of $^{5'RG}_{C}$. If the orientation of the GC pair is switched to CG ($^{5'RC}_{G}$), the 5′-P base has little stacking with either the intrastrand C base or the cross-strand G base. Presumably, the weaker stacking between a purine and a pyrimidine base is not sufficient to restrict the 5′-R base in a stacked state with the C base of the CG pair in this context.

Conversely, a purine base 3′ to a GC or UG pair has a significant population of overlap with the terminal pair. In these cases, the orientation of the terminal base pair is critical in determining the base of which strand the dangling base predominantly stacks upon (Figure 5). Typically, purine−purine stacking is more favorable than purine−pyrimidine stacking. Presumably the intrinsic flexibility of a 3′-dangling end base allows it to seek the conformation that is most favorable for base stacking (*12*). A 3′-dangling purine tends to have more cross-stranded stacking with the purine in the CG pair (*10*) but more intrastranded stacking with the purine in the GC pair (*6, 11*). Driven by stronger stacking interactions between larger purine bases, the dangling base can switch the stacking partner depending on the orientation of the terminal GC pair, thus providing different degrees of stabilization. Higher populations with cross-stranded stacking interactions provide more stabilization to the overall duplex stability than intrastranded stacking. More significantly, these results suggest that all of these context-dependent structural features

are dynamic and heterogeneous. The dangling bases exist in a dynamic equilibrium between stacked and unstacked conformations, and the population distributions resolved by the ultrafast dynamics strategy provide a structural basis for understanding the sequence-dependent thermodynamic stability. The added dynamic dimension to the structure−thermodynamics relationship significantly advances our understanding of the role of RNA conformational dynamics in modulating stability and functions.

It has been argued that RNA's unique thermodynamic properties might be well adapted for its possible role as the first macromolecules within the RNA world hypothesis (*50*). In particular, it has been noted that because a 3′-dangling end base contributes to the stability of a duplex more than a 5′-dangling end does, the elongation of an RNA chain is more energetically favored in a 5′- to 3′-direction in a prebiotic world when energy conservation is crucial. Our findings reported here provide a more precise structural basis of the thermodynamic advantages for assembly of RNA molecules in a 5′- to 3′-direction, lending further supporting evidence for RNA's evolutionary role.

In a number of cases, the sums of the stability contributions from the two corresponding 5′- and 3′-dangling ends are almost equal to the stability increments from a terminal base pair (*11, 12*), suggesting that base stacking is more dominant than hydrogen-bonding interaction in stabilizing RNA duplex structures and folding. For example, the stacking interactions are more important than base pairing interactions in determining the stability of the terminal AU base pairs in a ACCGGU duplex (*6*). It has been estimated that the stacking of a 3′-dangling A and a 5′-dangling U together contributes about 60% of the energetics toward a terminal AU pair adjacent to a GC pair in the context of $^{GA3'}_{CU5'}$ (*6, 10*). However, it is not clear whether the geometries of the separate dangling ends are the same as those involved in a terminal base pair between bases on opposite strands. It is possible that strong stacking interactions favor geometries that are not necessarily optimal for hydrogen-bonding interactions between the bases in a terminal pair (*11*). On the other hand, Watson−Crick or non-Watson−Crick hydrogen-bonding interactions between dangling end bases on opposite strands can modulate or alter the stacking interactions with the adjacent base pair, depending on the number or the strength of these hydrogen bonds (*15*). Specifically, hydrogen bonding between the 5′-base and the opposing 3′-base may drive the unstacked 5′-base into a stacked conformation.

Our dynamic probing of the P base in constructs where it can potentially form a pair with a U revealed interesting context-dependent differences in the stacking interactions between the 5′-dangling and 3′-dangling purine (Figure 5). Apparently, a 5′-U does not alter the nature of the interactions between a 3′-purine and the terminal GC pair, regardless of the orientation of the pair. This suggests that the stacking interactions involving the 3′-dangling purine base with the G in the GC/CG pair are dominant over the potential hydrogen-bonding interactions between the dangling R and U. The geometry of the terminal RU pair is optimized mostly for the stacking interactions, and the stacking interactions between the 3′-dangling R with the terminal GC pair remain intact. Presumably, altering the optimal base stacking interactions would result in unacceptable energetic penalty that cannot be compensated by the hydrogen-bonding interactions between the bases. On the other hand, formation of the RU pair drastically changes the conformations of the 5′-R. A 5′-R alone lacks significant stacking interactions compared to a 3′-R as discussed above. However, formation of hydrogen-bonding interactions between the 5′-R and an opposing 3′-U can drive the largely unstacked 5′-R into a largely stacked conformation, particularly when the 5′-R is adjacent to a G on the same strand (Figure 5); therefore, significant purine−purine stacking interactions can result from the hydrogen-bonding interactions. These observations point to the interplay of base stacking and hydrogen-bonding interactions in determining RNA secondary and tertiary structures in a strongly sequence-dependent manner.

By resolving heterogeneous structural populations of dangling end bases that are dynamically exchanging on fast time scales, we have elucidated the correlation between the dynamic conformational distributions and thermodynamic stability. These findings can also provide a basis for understanding the dynamic structural features of other RNA motifs that contain such ubiquitous stacking interactions between bases. For example, base stacking interactions are the major determinants for structural formation of bulges, coaxial stacking, multibranch junctions, etc., and play an important role in RNAi-mediated gene regulations. The unique feature and advantage of the ultrafast dynamics approach are that the heterogeneous conformations can be probed simultaneously and quantitatively with single-residue spatial resolution. This new tool should complement existing powerful traditional structural biology approaches, particularly NMR spectroscopy, single molecule approaches, and molecular dynamics simulations, that are heavily used in elucidating molecular motions in RNA. Information obtained from this research should be useful for interpretation of NMR data for testing multiple-conformational models and for directly comparing results from single molecule experiments and molecular dynamics simulations. The findings from this research, when integrated with those from the other methods, will provide unique insights into the principles of RNA folding, conformational dynamics, and its role in molecular recognition and function and improve our ability to predict RNA structures. Ultimately, such RNA structure prediction efforts will also include prediction of the dynamics from sequence and motif architectures.

ACKNOWLEDGMENT

We thank Dr. Mark E. Burkard for critical comments on the manuscript.

SUPPORTING INFORMATION AVAILABLE

One table of the complete thermodynamic parameters for the RNA constructs and core duplexes and four figures of femtosecond decay profiles for constructs. This material is available free of charge via the Internet at http://pubs.acs.org.

REFERENCES

1. Turner, D. H., Sugimoto, N., and Freier, S. M. (1988) RNA Structure Prediction. *Annu. Rev. Biophys. Biophys. Chem. 17*, 167–192.

2. Gennis, R. B., and Cantor, C. R. (1970) Optical Properties of Specific Complexes between Complementary Oligoribonucleotides. *Biochemistry 9*, 4714.
3. Martin, F. H., Uhlenbec, O. C., and Doty, P. (1971) Self-Complementary Oligoribonucleotides: Adenylic Acid-Uridylic Acid Block Copolymers. *J. Mol. Biol. 57*, 201–215.
4. Romaniuk, P. J., Hughes, D. W., Gregoire, R. J., Neilson, T., and Bell, R. A. (1978) Stabilizing Effect of Dangling Bases on a Short RNA Double Helix as Determined by Proton Nuclear Magnetic-Resonance Spectroscopy. *J. Am. Chem. Soc. 100*, 3971–3972.
5. Alkema, D., Bell, R. A., Hader, P. A., and Neilson, T. (1981) Triplet Gpcpa Forms a Stable RNA Duplex. *J. Am. Chem. Soc. 103*, 2866–2868.
6. Petersheim, M., and Turner, D. H. (1983) Base-Stacking and Base-Pairing Contributions to Helix Stability: Thermodynamics of Double-Helix Formation with CCGG, CCGGp, CCGGAp, ACCGGp, CCGGUp, and ACCGGUp. *Biochemistry 22*, 256–263.
7. Freier, S. M., Kierzek, R., Jaeger, J. A., Sugimoto, N., Caruthers, M. H., Neilson, T., and Turner, D. H. (1986) Improved Free-Energy Parameters for Predictions of RNA Duplex Stability. *Proc. Natl. Acad. Sci. U.S.A. 83*, 9373–9377.
8. Xia, T., SantaLucia, J., Burkard, M. E., Kierzek, R., Schroeder, S. J., Jiao, X., Cox, C., and Turner, D. H. (1998) Thermodynamic Parameters for an Expanded Nearest-Neighbor Model for Formation of RNA Duplexes with Watson-Crick Base Pairs. *Biochemistry 37*, 14719–35.
9. Xia, T., Mathews, D. H., and Turner, D. H. (2001) *Thermodynamics of RNA Secondary Structure Formation in RNA* (Soll, D., Nishimura, S., and Moore, P. B., Eds.) Elsevier Science, Oxford.
10. Freier, S. M., Burger, B. J., Alkema, D., Neilson, T., and Turner, D. H. (1983) Effects of 3′ Dangling End Stacking on the Stability of GGCC and CCGG Double Helices. *Biochemistry 22*, 6198–6206.
11. Freier, S. M., Alkema, D., Sinclair, A., Neilson, T., and Turner, D. H. (1985) Contributions of Dangling End Stacking and Terminal Base-Pair Formation to the Stabilities of XGGCCp, XCCGGp, XGGCCYp, and XCCGGYp Helixes. *Biochemistry 24*, 4533–4539.
12. Freier, S. M., Sugimoto, N., Sinclair, A., Alkema, D., Neilson, T., Kierzek, R., Caruthers, M. H., and Turner, D. H. (1986) Stability of XGCGCp, GCGCYp, and XGCGCYp Helixes—an Empirical Estimate of the Energetics of Hydrogen-Bonds in Nucleic-Acids. *Biochemistry 25*, 3214–3219.
13. Sugimoto, N., Kierzek, R., and Turner, D. H. (1987) Sequence Dependence for the Energetics of Dangling Ends and Terminal Base-Pairs in Ribonucleic-Acid. *Biochemistry 26*, 4554–4558.
14. Kool, E. T. (2001) Hydrogen bonding, base stacking, and steric effects in DNA replication. *Annu. Rev. Biophys. Biomol. Struct. 30*, 1–22.
15. Burkard, M. E., Kierzek, R., and Turner, D. H. (1999) Thermodynamics of Unpaired Terminal Nucleotides on Short RNA Helixes Correlates with Stacking at Helix Termini in Larger RNAs. *J. Mol. Biol. 290*, 967–982.
16. Guckian, K. M., Schweitzer, B. A., Ren, R. X. F., Sheils, C. J., Paris, P. L., Tahmassebi, D. C., and Kool, E. T. (1996) Experimental Measurement of Aromatic Stacking Affinities in the Context of Duplex DNA. *J. Am. Chem. Soc. 118*, 8182–8183.
17. Guckian, K. M., Schweitzer, B. A., Ren, R. X. F., Sheils, C. J., Tahmassebi, D. C., and Kool, E. T. (2000) Factors Contributing to Aromatic Stacking in Water: Evaluation in the Context of DNA. *J. Am. Chem. Soc. 122*, 2213–2222.
18. Ziomek, K., Kierzek, E., Biala, E., and Kierzek, R. (2002) The Influence of Various Modified Nucleotides Placed as 3′-Dangling End on Thermal Stability of RNA Duplexes. *Biophys. Chem. 97*, 243–249.
19. Rosemeyer, H., and Seela, F. (2002) Modified Purine Nucleosides As Dangling Ends of DNA Duplexes: The Effect of the Nucleobase Polarizability on Stacking Interactions. *J. Chem. Soc., Perkin Trans. 2*, 746–750.
20. Bommarito, S., Peyret, N., and SantaLucia, J. (2000) Thermodynamic Parameters for DNA Sequences with Dangling Ends. *Nucleic Acids Res. 28*, 1929–1934.
21. Quartin, R. S., and Wetmur, J. G. (1989) Effect of Ionic Strength on the Hybridization of Oligodeoxynucleotides with Reduced Charge Due to Methylphosphonate Linkages to Unmodified Oligodeoxynucleotides Containing the Complementary Sequence. *Biochemistry 28*, 1040–1047.
22. Mellema, J. R., Vanderwoerd, R., Vandermarel, G. A., Vanboom, J. H., and Altona, C. (1984) Proton NMR Study and Conformational Analysis of d(CGT), d(TCG) and d(CGTCG) in Aqueous Solution. The Effect of a Dangling Thymidine and of a Thymidine Mismatch on DNA Mini-Duplexes. *Nucleic Acids Res. 12*, 5061–5078.
23. Senior, M., Jones, R. A., and Breslauer, K. J. (1988) Influence of Dangling Thymidine Residues on the Stability and Structure of Two DNA Duplexes. *Biochemistry 27*, 3879–3885.
24. Limmer, S., Hofmann, H. P., Ott, G., and Sprinzl, M. (1993) The 3′-Terminal End (NCCA) of rRNA Determines the Structure and Stability of the Aminoacyl Acceptor Stem. *Proc. Natl. Acad. Sci. U.S.A. 90*, 6199–6202.
25. Ohmichi, T., Nakano, S., Miyoshi, D., and Sugimoto, N. (2002) Long RNA Dangling End Has Large Energetic Contribution to Duplex Stability. *J. Am. Chem. Soc. 124*, 10367–10372.
26. O'Toole, A. S., Miller, S., and Serra, M. J. (2005) Stability of 3′ Double Nucleotide Overhangs That Model the 3′ Ends of siRNA. *RNA 11*, 512–516.
27. O'Toole, A. S., Miller, S., Haines, N., Zink, M. C., and Serra, M. J. (2006) Comprehensive Thermodynamic Analysis of 3′ Double-Nucleotide Overhangs Neighboring Watson-Crick Terminal Base Pairs. *Nucleic Acids Res. 34*, 3338–3344.
28. Doktycz, M. J., Paner, T. M., Amaratunga, M., and Benight, A. S. (1990) Thermodynamic Stability of the 5′ Dangling-Ended DNA Hairpins Formed from Sequences 5′-$(XY)_2$GGATAC$(T)_4$GTATCC-3′, Where X, Y = A, T, G, C. *Biopolymers 30*, 829–845.
29. Riccelli, P. V., Mandell, K. E., and Benight, A. S. (2002) Melting Studies of Dangling-Ended DNA Hairpins: Effects of End Length, Loop Sequence and Biotinylation of Loop Bases. *Nucleic Acids Res. 30*, 4088–4093.
30. Isaksson, J., and Chattopadhyaya, J. (2005) A Uniform Mechanism Correlating Dangling-End Stabilization and Stacking Geometry. *Biochemistry 44*, 5390–5401.
31. Isaksson, J., Acharya, S., Barman, J., Cheruku, P., and Chattopadhyaya, J. (2004) Single-Stranded Adenine-Rich DNA and RNA Retain Structural Characteristics of Their Respective Double-Stranded Conformations and Show Directional Differences in Stacking Pattern. *Biochemistry 43*, 15996–16010.
32. Crothers, D. M. (2001) *RNA Conformational Dynamics in RNA* (Soll, D., Nishimura, S., andMoore, P. B., Eds.) Elsevier Science Ltd., Oxford.
33. Zhao, L., and Xia, T. (2007) Direct Revelation of Multiple Conformations in RNA by Femtosecond Dynamics. *J. Am. Chem. Soc. 129*, 4118–4119.
34. McDowell, J. A., and Turner, D. H. (1996) Investigation of the Structural Basis for Thermodynamic Stabilities of Tandem GU Mismatches: Solution Structure of $(rGAGGUCUC)_2$ by Two-Dimensional NMR and Simulated Annealing. *Biochemistry 35*, 14077–14089.
35. Fiebig, T., Wan, C., and Zewail, A. H. (2002) Femtosecond Charge Transfer Dynamics of a Modified DNA Base: 2-Aminopurine in Complexes with Nucleotides. *ChemPhysChem 3*, 781–788.
36. Holmen, A., Norden, B., and Albinsson, B. (1997) Electronic Transition Moments of 2-Aminopurine. *J. Am. Chem. Soc. 119*, 3114–3121.
37. Lakowicz, J. R. (1999) *Principles of Fluorescence Spectroscopy*, 2nd ed., Kluwer Academic/Plenum Plublishers, New York.
38. Wan, C., Fiebig, T., Schiemann, O., Barton, J. K., and Zewail, A. H. (2000) Femtosecond Direct Observation of Charge Transfer between Bases in DNA. *Proc. Natl. Acad. Sci. U.S.A. 97*, 14052–14055.
39. O'Neill, M. A., Becker, H. C., Wan, C., Barton, J. K., and Zewail, A. H. (2003) Ultrafast Dynamics in DNA-Mediated Electron Transfer: Base Gating and the Role of Temperature. *Angew. Chem., Int. Ed. Engl. 42*, 5896–5900.
40. Wan, C. Z., Xia, T. B., Becker, H. C., and Zewail, A. H. (2005) Ultrafast Unequilibrated Charge Transfer: A New Channel in the Quenching of Fluorescent Biological Probes. *Chem. Phys. Lett. 412*, 158–163.
41. Xia, T., Becker, H. C., Wan, C., Frankel, A., Roberts, R. W., and Zewail, A. H. (2003) The RNA-Protein Complex: Direct Probing of the Interfacial Recognition Dynamics and Its Correlation with Biological Functions. *Proc. Natl. Acad. Sci. U.S.A. 100*, 8119–8123.
42. Xia, T., Wan, C. Z., Roberts, R. W., and Zewail, A. H. (2005) RNA-Protein Recognition: Single-Residue Ultrafast Dynamical Control of Structural Specificity and Function. *Proc. Natl. Acad. Sci. U.S.A. 102*, 13013–13018.
43. Ganguly, M., Wang, F., Kaushik, M., Stone, M. P., Marky, L. A., and Gold, B. (2007) A Study of 7-Deaza-2′-deoxyguanosine-2′-deoxycytidine Base Pairing in DNA. *Nucleic Acids Res. 35*, 6181–6195.

44. Freier, S. M., Kierzek, R., Caruthers, M. H., Neilson, T., and Turner, D. H. (1986) Free-Energy Contributions of G·U and Other Terminal Mismatches to Helix Stability. *Biochemistry 25*, 3209–3213.

45. Akke, M., Fiala, R., Jiang, F., Patel, D., and Palmer, A. G. (1997) Base Dynamics in a UUCG Tetraloop RNA Hairpin Characterized by N-15 Spin Relaxation: Correlations with Structure and Stability. *RNA 3*, 702–709.

46. Zhang, Q., Sun, X. Y., Watt, E. D., and Al-Hashimi, H. M. (2006) Resolving the Motional Modes That Code for RNA Adaptation. *Science 311*, 653–656.

47. Pal, S. K., Zhao, L., Xia, T., and Zewail, A. H. (2003) Site- and Sequence-Selective Ultrafast Hydration of DNA. *Proc. Natl. Acad. Sci. U.S.A. 100*, 13746–13751.

48. O'Neill, M. A., and Barton, J. K. (2002) Effects of Strand and Directional Asymmetry on Base-Base Coupling and Charge Transfer in Double-Helical DNA. *Proc. Natl. Acad. Sci. U.S.A. 99*, 16543–16550.

49. Uhlenbeck, O. C. (1995) Keeping RNA Happy. *RNA 1*, 4–6.

50. Turner, D. H. (1993) *Thermodynamic Considerations for Evolution by RNA in The RNA World* (Gesteland, R. F., and Atkins, J. F., Eds.) Cold Spring Harbor Laboratory Press, Cold Spring Harbor, NY.

BI800210T